ASGE Vol. 05 (01), pp. 14-27, 2021

Egyptian Knowledge Bank

International Journal of Advances in Structural and Geotechnical Engineering

https://asge.journals.ekb.eg/

Print ISSN 2785-9509 Online ISSN 2812-5142

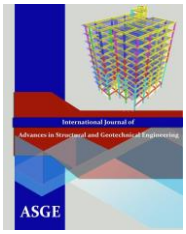

The effect of critical regions reinforcement on the flexural capacity and moment redistribution of RC continuous T-beams (Experimental and Numerical study)

Hesham Diab[1], Mohamed Rashwan[2], Tarek Abdelaleem[3]

[2]*Associate Professor, Faculty of Engineering, Assiut University, Egypt*
E-mail: Hesham Diab2@yahoo.com
[3]*Professor, Faculty of Engineering, Assiut University, Egypt*
[1]*Assistant Professor, Faculty of Engineering, Assiut University, Egypt*
E-mail: TarekAbdelaleem@aun.edu.eg

ABSTRACT

Despite linear analysis in several design codes for concrete structures, with re-distribution of moment in RC continuous beams. However, in deciding the importance of moment redistribution ratio in these codes and its meaning in the design, there is a strong mismatch due to ignoring several variables that have a direct effect on the load carrying capacities and the serviceability limits, which in turn leads to very conservative or unsafe designs. This paper aims at developing models of 3D nonlinear finite elements (FE) and investigating numerically the influence of the tensile reinforcement of sagging and hogging region on the performance of the RC continuous T-beams and their effect on the moment redistribution by using three experimental specimens for verification. The three two-span RC continuous beams were manufactured and tested up to failure, and designed with a loaded central concrete column. The results show that the sagging reinforcement improves the ductility and the serviceability of the continuous beams at the allowable deflection and the permissible crack width. The moment redistribution ratio depends on the ratio between the sagging reinforcement and the hogging reinforcement areas. At the hogging and sagging regions with equal reinforcement areas, the momentum redistribution ratio is low, regardless of the reinforcement ratio.

Keywords: continuous beams, moment redistribution, sagging and hogging region, , FEM.

INTRODUCTION

In previous years, the majority of the experimental research was carried out on the simple beams, whether to study the behaviour under vertical loads, the influence of the concrete compressive strength, the form of longitudinal and transverse reinforcement or to study the strength of beams due to defects in the design, implementation or environmental conditions by using steel plates or FRP material [1-7]. Few researches have studied the behaviour of the RC continuous beams [8 -11], despite the importance of the RC continuous beams in the vital structures such as concrete bridges, factories, …etc., and it is most likely to act as main components. Over the last few years, there has been a focus on studies of the flexural performance of the strengthened RC continuous beams under vertical loads [12-17], the effect of the strengthening method on the moment redistribution ratio, and the efficiency by using the external

prestressing system [18-23]. It was noted that the majority of the constructed continuous beams are supported on columns ,unlike the previous researches, which had steel plates as supports. Previous researches did not concern on the effect of main steel reinforcement at each critical section on the efficiency and behaviour of RC continuous beams in yield loads or service loads. Whereas, the load-carrying capacity of the RC continuous beam does not depend on the reinforcement of the one critical section. moreover, these studies focused on the effect of reinforcement ratios on the moment redistribution between the critical sections .There is, however, still a certain lack of consensus regarding the value of the redistribution coefficients [24-26], because of the clear difference in these values. Therefore, this study aims at investigating the behaviour of RC continuous T-beams when varying the area of the longitudinal reinforcement at the hogging or the sagging region and with a central loaded column, the effect of this variation on the moment redistribution ratio and the effect of central loaded columns on the performance of the statically indeterminate beams.
Furthermore, for numerically simulating the behaviour of tested specimens, an incremental nonlinear displacement-controlled 3D finite element (FE) analysis was used. Concerning the load-deflection, redistribution of moment, load-crack width relationships, load-carrying capacity and modes of failure for tested beams, similarities between the FE predictions and experimental results showed very strong alignment. The model predictions, as a whole, are in reasonable agreement with experimental results.

Summary of experimental program.

In the research of [24 and 25], descriptions of the experimental study can be found. Three RC continuous T-beams [BS1, BS2, and BS3] were designed to fail in flexural as shown in **Table 1.** The dimensions and reinforcing of the tested beams are shown in **Figure 1**. All RC continuous beams were designed to fail due to steel yielding at both mid-span and middle support sections.
By prestressing a 25 mm deformed bar, the central columns were loaded by about 120 kN as a constant load before loading the beams.

Table 1. Compressive strength for the tested beams and reinforcement arrangement:

Beam	f_{cu} (MPa)	Length m	Steel shear stirrups	Bottom RFT.		Top RFT.	
				Reinforcement	Ratio %	Reinforcement	Ratio %
BS1	28.0	4.30	Φ8@100 mm	2ϕ12	0.43	2ϕ12	0.43
BS2	27.5			2ϕ16	0.77	2ϕ12	0.43
BS3	36			2ϕ16	0.77	2ϕ12+2 ϕ10	0.74

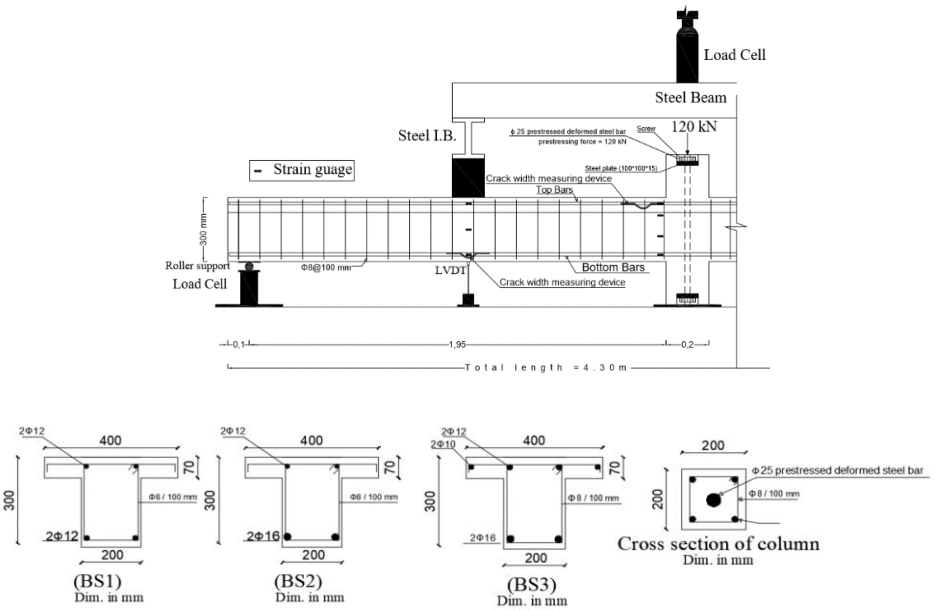

Fig. 1. Series of tested beams and the middle column.

The central support was the loaded column for all the tested beams, so the two load cells were used at the end supports to record the end reactions and thus calculate the experimental moments. Also, for all beams, the LVDTs were used under point load in the middle of each span to measure the deflections as shown in **Figure 1**. Additionally, crack width gauges were installed in the middle of each span to record the crack width at the sagging region. A 5,000-kN hydraulic machine was used to apply concentrated load on a stiff steel beam that in turn transmitted the load to the midpoint of each span. The load applied on each span was then evenly transferred to the beam by the associated steel beam. Readings of all instrumentations were acquired and stored using a data logger (TDS 150) system monitored by a computer. The measured initial crack, yield and ultimate loads of test specimens are shown in **Table 2**.

Table 2. Experimental results at cracking, service yield and ultimate loads of test specimens.

Beam Specimen	P_{cr}		P_y		kN.m$M_{y(exp.)}$		P_u	kN.m$M_{u(exp.)}$		Failure mode
	Hogging region	Sagging region	Hogging region	Sagging region	Hogging region	Sagging region		Hogging region	Sagging region	
BS1	81.25	71	195	202	42.26	33.3	251.25	47.94	34.81	conventional ductile flexural failure
BS2	76.88	63.8	260	278.03	42.35	48.94	347.22	45.21	58.78	
BS3	92.75	84	306.25	317.5	42.35	52.58	362.25	73.11	56.31	

Experimental results and discussion.

General behaviour, cracking pattern and failure mode

The cracking pattern for all beams is shown in **Figure 3**. The traditional ductile flexural failure occurred for all beams as a result of yielding of the longitudinal tensile steel reinforcement, followed by concrete crushing at the central support and the mid-span sections. Strain measurements of tensile steel in middle support and mid-span regions of the tested beams uncovered that, as expected, a plastic hinge was formed firstly upon the yielding of the upper tensile steel in the hogging region. After the yield of the hogging tensile steel, expansion of the flexural cracks, the rotation of the beam in this region, and redistribution of moments occurred from the central support toward the positive moment region of the beam. Once yielding of the bottom reinforcement, the concrete at the compression regions reached to its ultimate crushing strain. The modes of failure for all tested beams are shown in **Figures 4**, **5**, and **6**. The cracking patterns for the tested beams at failure are shown in **Figure 3**. In these figures, the following is observed:

BS1 The beam, BS, showed fewer cracks with larger spacing compared to the others. Before the steel yielding, the shear cracks began to appear at the shear spans, these cracks propagated and distributed regularly along two-beam spans.The shear crack was formed after the steel yielding. the distances between the cracks were from [150:200] mm. The cracks width increased dramatically after the steel yielding while the load capacity slowly increased until the beam failure. The observed mode of failure was yielding the top and bottom steel bars at the maximum moment regions at loads 195 kN and 202 kN respectively, which equal 78% and 80% of the ultimate load, and therefore the yielding of the main steel caused the formation of plastic hinges at the central support and at the spans of this beam, which was able to increase the deformation, followed by concrete crushing at the ultimate load. See **Figures 3** and **4.**

BS2 The flexural crack at the mid-span region began to spread toward the flange at load 64 kN, while the flexural shear crack started to form at load 200 kN. At the hogging region, the flange was completely cracked at load 135 kN (43.5 % of its ultimate load). The shear crack which was close to the end support at load 260 kN, however the flexural shear crack at the central support was at 240 kN. The negative cracks spread even 600 mm from the centre of the middle support.

BS3 Although the cracks concentrated at the maximum moment regions like the beam BS. At load 96 and 170 kN, the cracks extended at the sagging and hogging region respectively. It is also a

noticeable increase in the number of cracks at the central support region and the flexural failure was clearly shown without influential shear cracks in the failure mode.

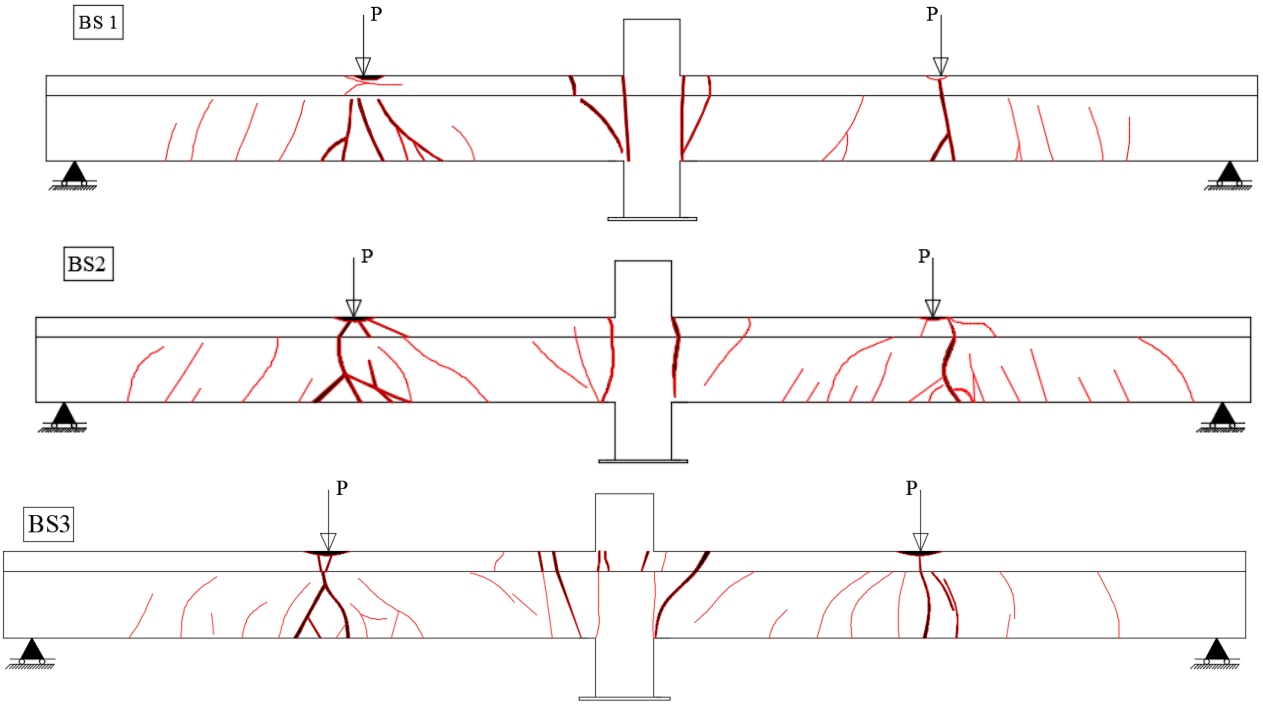

Fig. 3. Cracking patterns of the tested continuous beams.

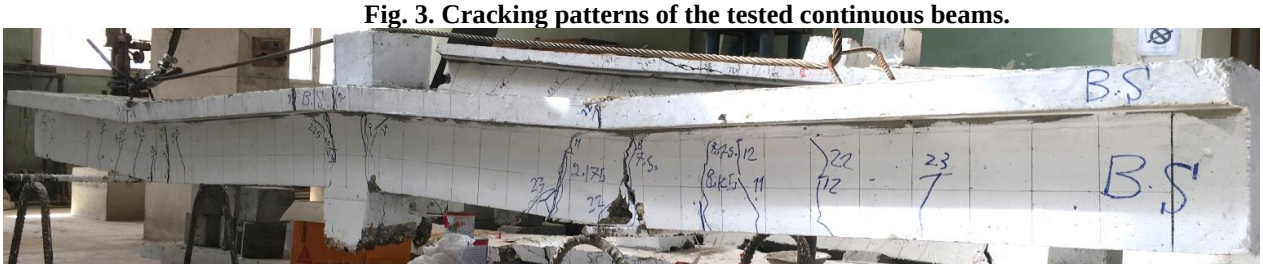

Fig. 4. Failure mode of beam BS1.

Fig. 5. Failure mode of beam BS2.

Fig. 6. Failure mode of beam BS3.

Figures 7 and **8.** Show the total applied load versus flexural crack width at the hogging and sagging regions respectively. in general, the crack width in the critical sections was affected by varying the reinforcement area at the both critical regions, especially after the steel yielding. The hogging moment regions showed a clear smaller crack width compared to that of the sagging moment regions, where the

crack widths at the positive moment regions were equal more than three times of those in the hogging moment regions especially for the beams BS2 and BS3. For the beam BS1, the crack widths were 0.5mm at both critical regions before the steel yielding, these widths developed dramatically to reach 3.4 mm and 6.2 mm at the ultimate load for the hogging and the sagging regions respectively. On the other hand, the beams BS2 and BS3 continued to control the crack widths up to steel yielding and up to failure especially at the hogging region, where the crack width increased from 0.7 mm to 2.0 mm at the hogging region, due to redistribute the internal forces to the sagging region.

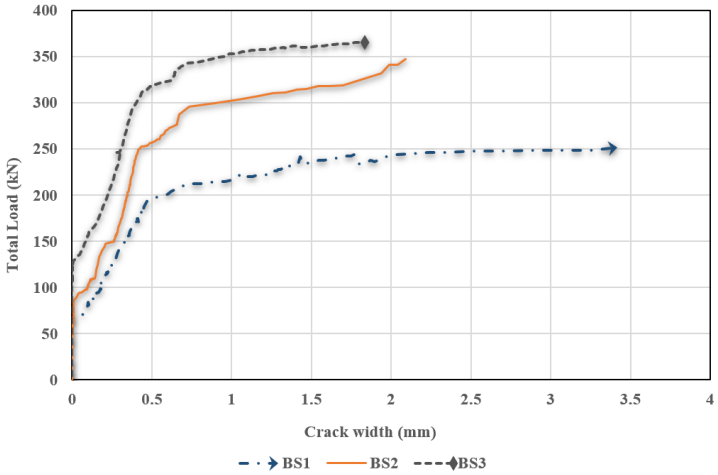

Fig. 7. Load–crack width relationship at the hogging moment region.

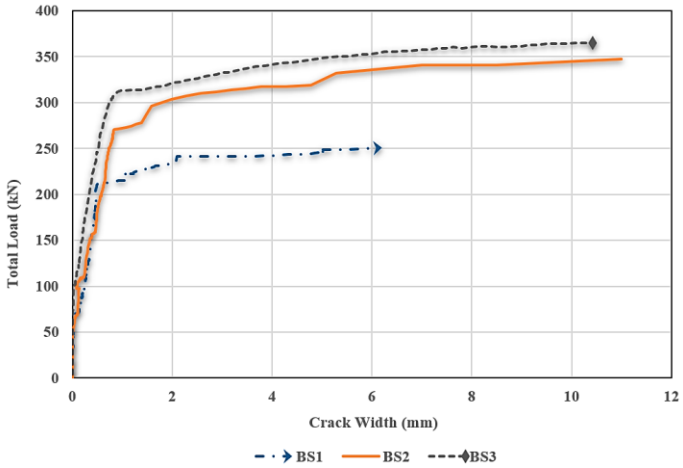

Fig. 8. Load–crack width relationship at the sagging moment region.

The relationship between the applied load and mid-span deflection for all tested beams is shown in **Figure 9**. The reinforcement ratio at the sagging and hogging region affected the stiffness of the beam specimens, also on the load-deflection curve. The beam BS1 was completely different after cracking load, due to the lower axial stiffness of the mid-span section than the others, a third stage that started after yielding of the top reinforcement had an increase in load with lower rate until the failure, as it could be seen in **Figure 9.**

Oppositely, because of increasing the bottom reinforcement by about 78 %, the same behaviour for the beams BS2 and BS3 has been observed because they had the same bottom reinforcement which has a major effect on the flexural stiffness of the beams. So, the load-deflection curve was less steep from beam BS1 at the post-cracking stage. So, the sagging reinforcement bars showed an essential role in resisting load after yielding of steel. Besides, these beams demonstrated ductile behaviour before failure, attributable to the enhancement of the sagging reinforcement. Overall, the type of the sagging reinforcement is a key factor in the value of the beam deflection while the hogging reinforcement played an influential role after the beam yield loads.

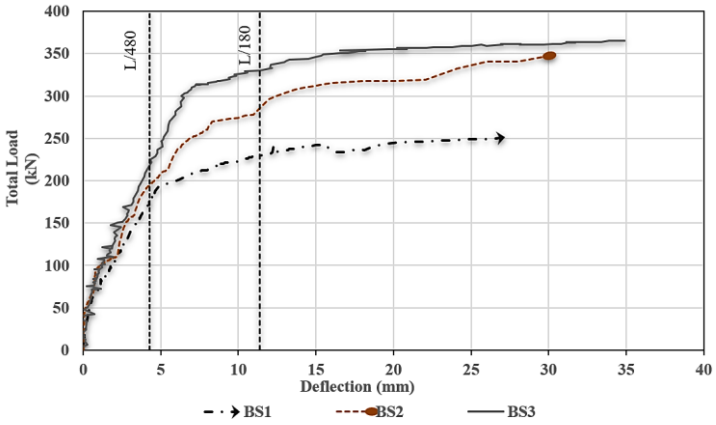

Fig. 9. Load-deflection relationship for the tested beams.

Finite element (FE) modeling

The numerical analysis research in this study is listed in this section. To simulate the flexural behaviour of continuous concrete beams reinforced with steel or hybrid bars, a non-linear finite element model (FEM) was constructed. In this method, the finite element analysis software package available for academia, ANSYS (ANSYS 2018.1), was used. To check the accuracy of the established FEM, the experimental results presented in the previous analysis were used.

The steps for constructing the FEM are discussed in detail, including the elements used in modeling, material types and boundary conditions. Furthermore, the various assumptions made in the finite element modeling process, including meshing, concrete constitutive models and the solution method used, are also discussed. The FEM was able to simulate with fair precision the behavior of the tested continuous concrete beam, and, despite the difficulties of convergence in the program solution, it was able to predict the post-failure behavior of concrete once failure started.

1.1. Material Properties and Elements Types

In this analysis, concrete was modeled using solid elements of three-dimensional eight-nodes. For the modeling of concrete, the solid element, SOLID65, was used. The key aspect of this element is the capacity to allow for material nonlinearity. This element will take into account cracking, plastic deformation and crushing in three perpendicular directions, as shown in **Figure 10**. In order to properly model concrete, SOLID 65 elements require linear isotropic and multi-linear isotropic material properties [26].

To define the concrete material, the modulus of elasticity (E_c) and the Poisson`s ratio have to be identified. In this study, the Poisson`s ratio was assumed to be 0.2 and the modulus of elasticity was calculated based on the following equation.

$$E_c = 4500\sqrt{f_{c`}} \qquad (1)$$

Where $f_{c`}$ is the maximum cylinder compressive strength.

Normal strength concrete's stress-strain relationship in compression usually consists of two parts; an ascending branch and a descending branch. However, in ANSYS software, the use of the ideal stress-strain curve with the descending branch contributes to problems with convergence. The descending branch of the concrete material model in ANSYS was, therefore, ignored in this review, as recommended in previous studies [27 :30]. The following equations were used to model the ascending branch of the multi-linear isotropic stress-strain curve for the concrete [31].

$$f_c = \begin{cases} f_{c`}\left(\left(\frac{2\varepsilon_c}{0.002}\right) - \left(\frac{\varepsilon_c}{0.002}\right)^2\right) & for \quad \varepsilon_c < 0.002 \qquad (16) \\ f_{c`} & for \ 0.002 \le \varepsilon_c \le 0.0035 \qquad (17) \end{cases}$$

Where:

f_c = stress (in MPa) at any strain;
ε_c = strain at stress f;

Based on the experimental specimens, the shear transfer coefficients for open and closed crakes were taken as 0.3 and 0.5. The stress of uniaxial cracking was based on the rupture modulus and was determined using the following equation.

$$f_r = 0.62\sqrt{f_{c`}} \qquad (19)$$

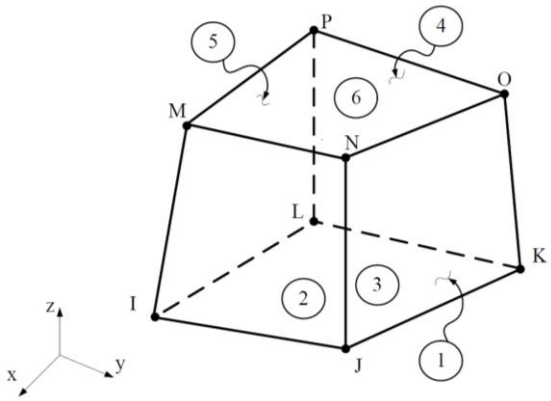

Fig. 10. Element SOLID 65 (reproduced from user manual ANSYS 2018).

In this study, the reinforcement materials (longitudinal bars and stirrups) have been modelled as truss elements with one node at each end. To that end, the LINK180 finite element was used. There are three degrees of freedom in the end nodes of this element, translation in the nodal directions of x, y and z. **Figure 11** shows the geometry and nodes of this element.

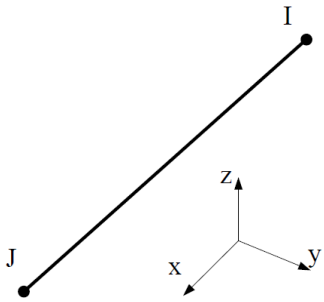

Fig. 11. LINK180 finite element (reproduced from user manual ANSYS 2018).

The LINK180 element requires linear isotropic and bi-linear isotropic material properties to be described to properly model steel reinforcement. The same element was specified instead with linear-elastic material properties in order to model FRP reinforcement. For steel reinforcement and FRP, the Poisson ratio was assumed to be 0.3 and 0.2 respectively. As discussed earlier, the modulus of elasticity for reinforcement materials was obtained experimentally.

The steel bearing plates used to distribute concentrated stresses at supports and loading points were also modeled. For this reason, the SOLID45 finite element was used. The steel bearing plates were constructed as a linear-elastic material with a 200 GPa and 0.3 Poisson elastic modulus.

ANSYS Model Geometry and Boundary Conditions

In geometry, loading and internal reinforcement, all tested beams are symmetric in the longitudinal direction around the middle support position. The cross-section of the beams tested is also symmetrical to the vertical axis that passes through center of gravity of the cross-section. Just one-quarter of the beam was modeled in ANSYS, using two-axis symmetry.

. Documented experimental studies confirm that the application of the column axial load increases to some extent the confinement effect of the beam-column joint region and contributes to an improvement in the joint's shear strength [32], as shown in **Figure 12.**

.

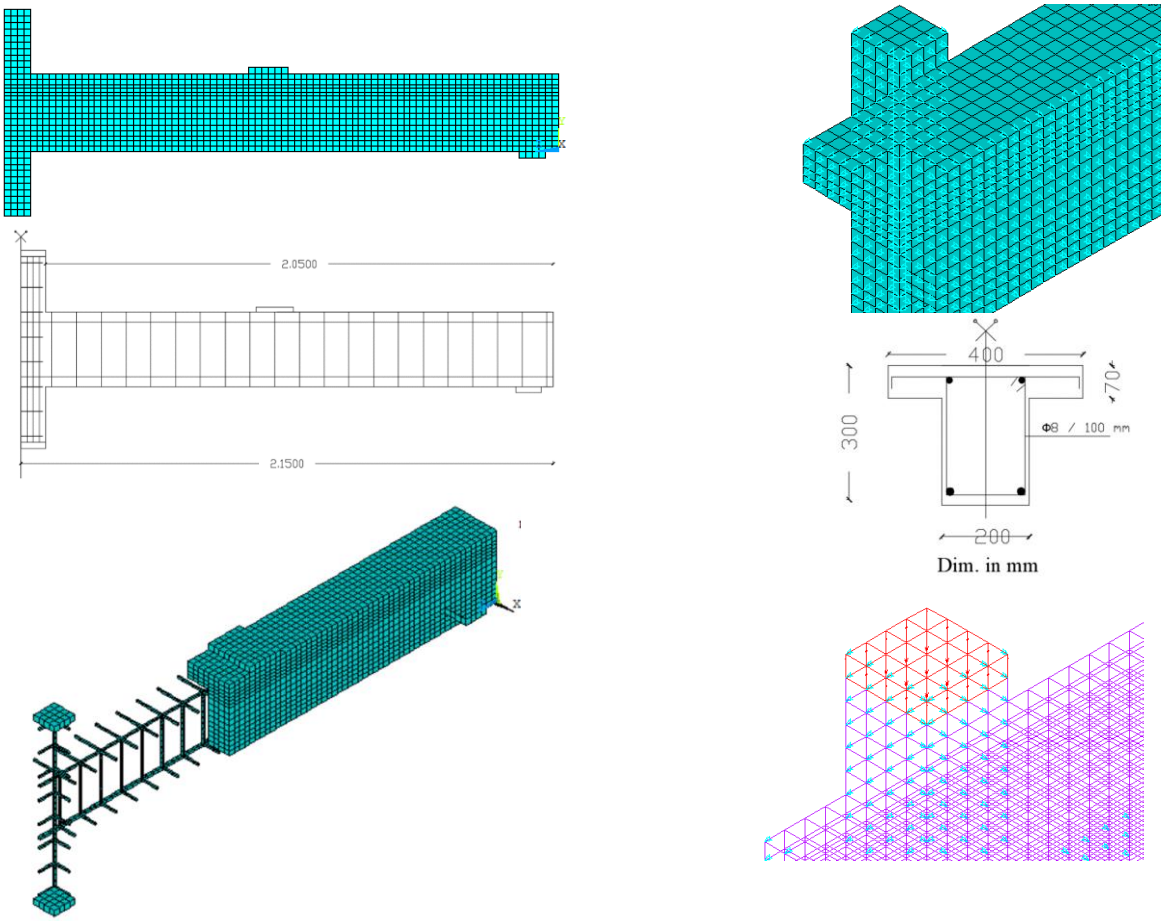

Fig. 12. Symmetry axes and boundary conditions

In order to have a minimal impact on the results and simulate the behavior of the tested beams with the highest possible precision, the size of the mesh used in the model was carefully selected. In order to determine the impact of mesh size on the finite element effects, a preliminary study was performed. The primary aim was to find the optimal mesh size to achieve a fair balance between the outcome accuracy and the number of nodes in the model, which significantly affects the necessary computing space and the processing time to solve the model. This is because, when omitted from the global stiffness matrix, cracked elements in coarse mesh cause issues. The use of smaller mesh sizes improved the model's accuracy and decreased the gap in performance, but it required a greater number of nodes. In the model, a 3D mesh size of 25 mm was adopted to save computing time. In finite element analysis, the overall applied load is separated into a sequence of load steps to take into consideration the influence of non-linearity.

Finite element results and discussion

Figure 13 shows the load-deflection behaviour of the steel-reinforced beams BS, CB, and C4 predicted by the FEM analysis against the experimental results. It can be seen that the FEM was able to demonstrate a similar response to the tested beams. The reduction of stiffness after cracking as well as the effect of steel yielding prior to failure was predicted by the models with a reasonable accuracy.

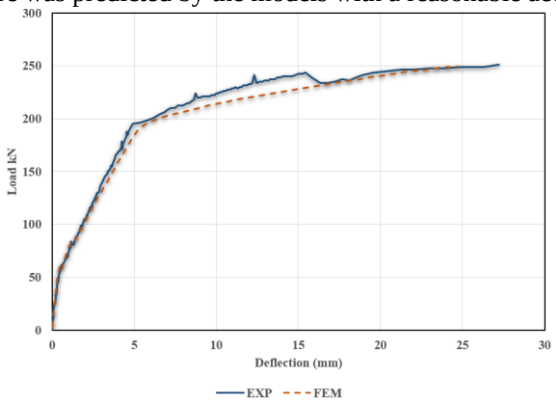

(a) BS1

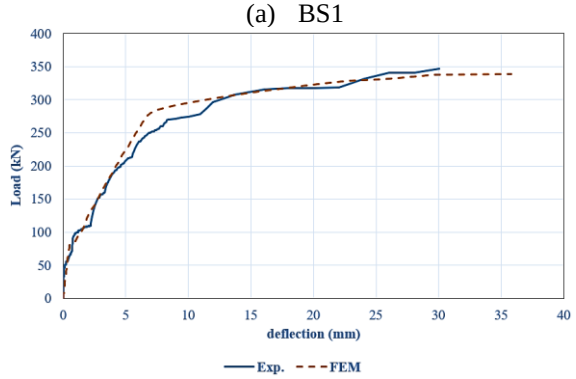

(b) BS2

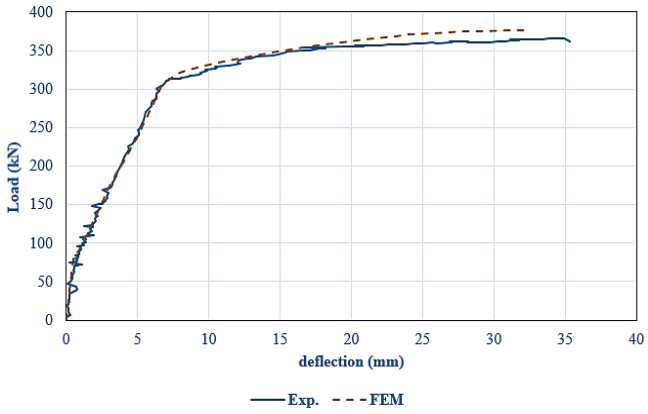

(c) BS3

Fig. 13 . Load-deflection behaviour of beams.

Since the problem is statically indeterminate, the predicted and experimental end reactions were compared to evaluate the ability of the model to redistribute bending moments. **Figure 14** shows the relationship between total applied load and end reactions for both experimental and ANSYS results. Again, a good agreement can be seen between the predicted and experimental results. These reaction results from ANSYS were used to calculate the bending moment at middle support section with different applied loads. The bending moments predicted by ANSYS are compared to the elastic bending moment at the same critical section (0.188 $P\ell$, where P is the applied load and ℓ is the beam span) to calculate the moment redistribution percentage at middle support. The relationship between moment redistribution and

applied load is then plotted and compared with the same relationship determined experimentally as shown in the following sections.

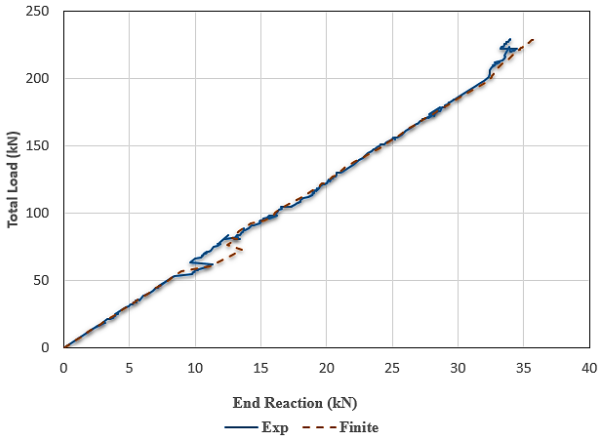

(a) BS1

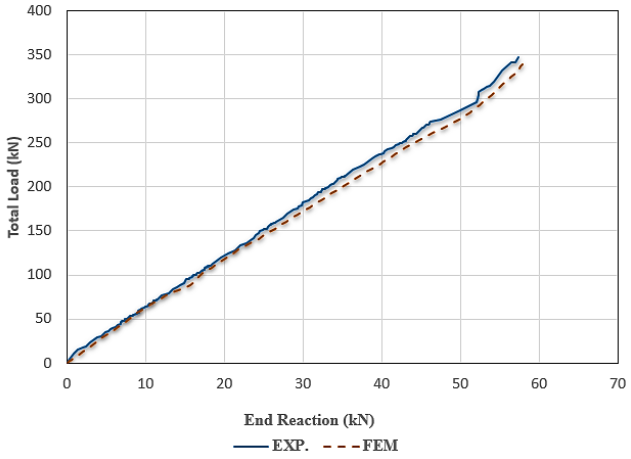

(b) BS2

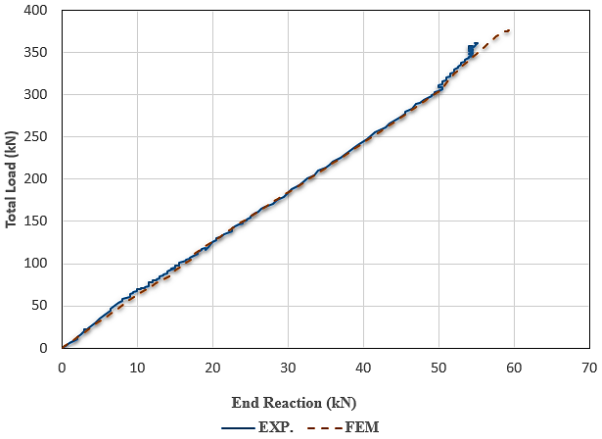

(C) BS3

Fig. 14. Load versus end reactions of steel beams.

The model was able to redistribute bending moments between critical sections. The relationship between the percentage of moment redistribution at the middle support section and the applied load are illustrated in **Figure 15.** It can be seen that the finite element model demonstrated significant moment redistribution

right after cracking. This percentage increased as the load increased all the way up to yielding loads. The predicted moment redistribution was within a range of 20% difference from experimental results.

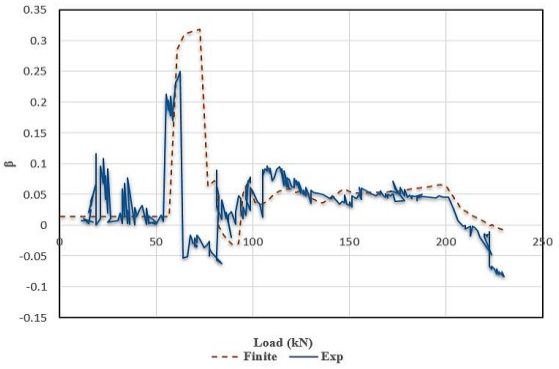

(a) BS1

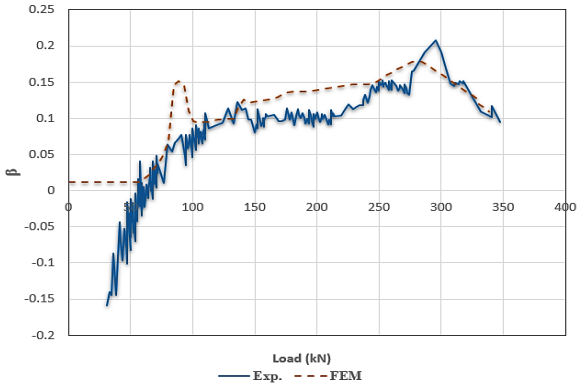

(b) BS2

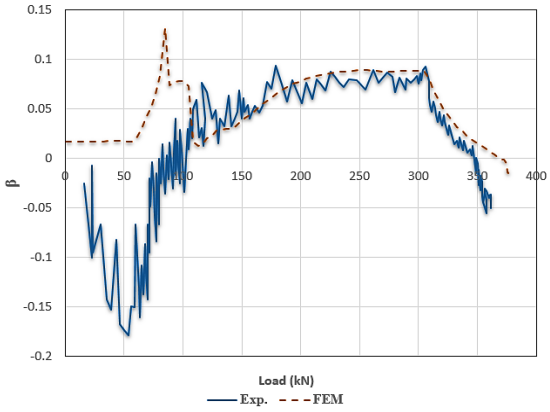

(c) BS3

Fig. 15. Load versus moment redistributions at middle support of beams.

Table 3 shows the comparison between the Experimental and FEM results at yield and ultimate loads for the specimens. As shown in this table, the finite element models predicted the yield and ultimate loads of the tested beam accurately. the difference between predicted and experimental loads was within 2%.

Table 3: comparison between the Experimental and FEM results at yield and ultimate loads.

Beam specimen	Yielding load at hogging region (kN)			Yielding load at sagging region (kN)			Ultimate load (kN)		
	Exp.	FEM	Exp./FEM	Exp.	FEM	Exp./FEM	Exp.	FEM	Exp./FEM
BS1	195	185	51.0	202	196.1	31.0	251.25	249.4	11.0
BS2	260	252	31.0	278.03	280.4	90.9	347.22	338.5	1.03
BS3	306.25	320.7	50.9	317.5	332.7	0.95	362.25	376.3	0.96
average	—	—	1.01	—	—	0.99	—	—	1.0

Conclusions and Recommendations

Experimental work was carried out on three large-scale RC continuous T-beams, to study the effect of main longitudinal reinforcement on the general behaviour of the tested beams and their ability to redistribute bending moment between hogging and sagging regions under the influence of vertical loads. Based on the test results and the comparisons between the tested beams which was presented in advance in this research we can draw the following conclusions:

1. The ultimate load capacity, service loads and flexural rigidity are affected by the sagging main reinforcement significantly.
2. The top reinforcement area had influence on the moment redistribution in RC continuous concrete beams even before reaching the yield load, and the hogging moment redistribution over the middle support is always larger than that at the mid-span because the stiffness of the middle section was lower than the mid-span region, where the flange was fully cracked before the yielding loads.
3. The formation of the plastic hinge at the mid-span region depends mainly on the ratio between upper and lower reinforcement, where increasing the lower reinforcement area compared to the upper reinforcement leads to formation the plastic hinge after the ultimate load and this helps to improve the ductility of the beam and give an amble warning before failure.
4. The FEM described in this chapter was able to predict with reasonable accuracy the load-deflection behaviour in addition to the available moment redistribution. Hence, the FEM can be used to conduct a parametric study to extend the range of the investigated parameters to better understand their influence on the behaviour of continuous RC T-beams. The results of this parametric study are presented in the following chapter.

REFERENCES

1. Saadatmanesh H, Ehsani MR. RC beams strengthened with GFRP plates. I: Experimental study. Journal of Structural Engineering; 117(11): 3417–33. 1991.
2. Jaeger, L. G., Tadros, G., and Mufti, A. A. (1995). Balanced section, ductility and deformability in concrete with FRP reinforcement. Res. Rep., Joint U.S. Can Meeting at West Virginia Univ., Morgantown, W. Va.
3. Grace NF, Soliman AK, Abdel-Sayed G, Saleh KR. Behavior and ductility of simple and continuous FRP reinforced beams. Journal of Composites for Construction, ASCE; 2(4):186–94. 1998.
4. De Lorenzis L, Teng JG. Near-surface mounted FRP reinforcement: an emerging technique for strengthening structures. Composites: Part B; 38:119–43. 2007.
5. Sharaky IA, Torres L, Baena M, Vilanova I. Effect of different material and construction details on the bond behaviour of NSM FRP bars in concrete. Construction and Building Materials; 38:890–902. 2013.

6. Obaydullah M., Jumaat M. Z., Alengaram U. J., Darain Kh. M. ud, Md. Nazmul Huda, Hosen Md. Akter. Prestressing of NSM steel strands to enhance the structural performance of prestressed concrete beams. Construction and Building Materials 129, 289–301. 2016.
7. Diab Hesham M. , Farghal Omer A. Bond strength and effective bond length of FRP sheets/plates bonded to concrete considering the type of adhesive layer. Composites Part B: Engineering Volume 58, March 2014, Pages 618-624.
8. Niklas Bagge, Alan O'Connor, Lennart Elfgren and Claus Pedersen. Moment redistribution in RC beams – A study of the influence of longitudinal and transverse reinforcement ratios and concrete strength. Engineering Structures 80 (2014) 11–23.
9. Carmo NFC, Lopes SMR. Available plastic rotation in continuous high-strength concrete beams. Journal of Civil Engineering. 2008; 35(10):1152–62.
10. Bigaj AJ. Structural dependence of rotation capacity of plastic hinge in RC beams and slabs. PhD Thesis. Delft: Delft University; (1999). 230 pages.
11. Shakir A. Moment redistribution in reinforced concrete structures. PhD Thesis. Edmonton: University of Alberta; (2005). 566 pages.
12. Ashour A.F., El-Refaie S.A., Garrity S.W. Flexural strengthening of RC continuous beams using CFRP laminates. Cement & Concrete Composites 26 (2004) 765–775.
13. Liu I. S. T., Oehlers D. J., and Seracino R. Tests on the ductility of reinforced concrete beams retrofitted with FRP and steel near-surface mounted plates. Journal of Composites for Construction © ASCE. 2006.10:106-114.
14. M.A. Aiello, L. Valente, A. Rizzo, Moment redistribution in continuous reinforced concrete beams strengthened with carbon-fiber-reinforced polymer laminates, Mechanics of Composite Materials 43(5) (2007) 453-466.
15. H. Akbarzadeh and A.A. Maghsoudi. Experimental and analytical investigation of reinforced high strength concrete continuous beams strengthened with fiber reinforced polymer. Materials and Design 31 (2010) 1130–1147.
16. A.A. Maghsoudi, H. Akbarzadeh Bengar. Acceptable lower bound of the ductility index and serviceability state of RC continuous beams strengthened with CFRP sheets. Scientia Iranica, Transactions A: Civil Engineering 18 (2011) 36–44.
17. Farhang Farahbod, Davood Mostofinejad. Experimental study of moment redistribution in RC frames strengthened with CFRP sheets, Composite Structures 93 (2011) 1168–1177.
18. Marco Andrea Pisani. Numerical Analysis of Continuous Beams Prestressed with External Tendons. J. Bridge Eng. 2009.14:93-101.
19. Ahmed Ghallab. Calculating ultimate tendon stress in externally prestressed continuous concrete beams using simplified formulas. Engineering Structures 46 (2013) 417–430.
20. Tiejiong Lou, Sergio M. R. Lopes and Adelino V. Lopes. Flexural Response of Continuous Concrete Beams Prestressed with External Tendons. Journal of Bridge Engineering © ASCE. 2013.18:525-537.
21. Ahmed Ghallab. Ductility of Externally Prestressed Continuous Concrete Beams. KSCE Journal of Civil Engineering (2014) 18(2):595-606.
22. Tiejiong Lou, Sergio M.R. Lopes and Adelino V. Lopes Factors affecting moment redistribution at ultimate in continuous beams prestressed with external CFRP tendons. Composites: Part B 66 (2014) 136–146.
23. J.S. Du, Francis T.K. Au, Enoch K.H. Chan and L. Liu. Deflection of unbonded partially prestressed concrete continuous beams. Engineering Structures 118 (2016) 89–96.
24. Diab H.M.A., Abdelaleem T., Rashwan M. M.M. Moment redistribution and flexural performance of RC continuous T-beams strengthened with NSM FRP or steel bars. Structures 28 (2020) 1516–1538.
25. Diab H.M.A., Abdelaleem T., Rashwan M. M.M. experimental investigation of Moment redistribution in RC continuous beams with t-cross section considering central loaded support. International Journal of Civil Engineering and Technology (IJCIET), 11(7), (2020) pp. 114-130.
26. ANSYS Mechanical Enterprise. A finite element computer software and user manual for nonlinear structural analysis. Mechanical APDL Release 18.1 UP20170403.

27. Kachlakev, D., Miller, T., Yim, S., Chansawat, K. and Potisuk, T. “Finite Element Modeling of Reinforced Concrete Structures strengthened with FRP Laminates.” Final Report SPR-316, Oregon Department of Transportation, Salem, Oregon (2001).
28. Wolanski, A. J. “Flexural Behavior of Reinforced and Prestressed Concrete Beams using Finite Element Analysis,” M.Sc. Thesis, Marquette University, Milwaukee, Wisconsin (2004).
29. Gorji, M. S. “Analysis of FRP Strengthened Reinforced Concrete Beams using Energy Variation Method,” World Applied Sciences Journal, 6(1), 105-111. (2009)
30. Büyükkaragöz, A. “Finite Element Analysis of the Beam Strengthened with Prefabricated Reinforced Concrete Plate,” Scientific Research and Essays, 5(6), 533-544. (2010).
31. Egyptian Code of Practice for Design and Construction of Concrete Structures ECCS 203-(2017).
32. Quintero-Febres CG, Wight JK. Experimental study of reinforced concrete interior wide beam–column connections subjected to lateral loading. ACI Structural Journal. 98:572–82. (2001).